JACS
JOURNAL OF THE AMERICAN CHEMICAL SOCIETY
Article
pubs.acs.org/JACS

Controlling Carrier Densities in Photochemically Reduced Colloidal ZnO Nanocrystals: Size Dependence and Role of the Hole Quencher

Alina M. Schimpf, Carolyn E. Gunthardt, Jeffrey D. Rinehart, James M. Mayer, and Daniel R. Gamelin*

Department of Chemistry, University of Washington, Seattle, Washington 98195-1700, United States

Supporting Information

ABSTRACT: Photodoped colloidal ZnO nanocrystals are model systems for understanding the generation and physical or chemical properties of excess delocalized charge carriers in semiconductor nanocrystals. Typically, ZnO photodoping is achieved photochemically using ethanol (EtOH) as a sacrificial reductant. Curiously, different studies have reported over an order of magnitude spread in the maximum number of conduction-band electrons that can be accumulated by photochemical oxidation of EtOH. Here, we demonstrate that this apparent discrepancy results from a strong size dependence of the average maximum number of excess electrons per nanocrystal, $\langle n_{max} \rangle$. We demonstrate that $\langle n_{max} \rangle$ increases in proportion to nanocrystal volume, such that the maximum carrier density remains constant for all nanocrystal sizes. $\langle n_{max} \rangle$ is found to be largely insensitive to precise experimental conditions such as solvent, ligands, protons or other cations, photolysis conditions, and nanocrystal or EtOH concentrations. These results reconcile the broad range of literature results obtained with EtOH as the hole quencher. Furthermore, we demonstrate that $\langle n_{max} \rangle$ depends on the identity of the hole quencher, and is thus not an intrinsic property of the multiply reduced ZnO nanocrystals themselves. Using a series of substituted borohydride hole quenchers, we show that it is possible to increase the nanocrystal carrier densities over 4-fold relative to previous photodoping reports. When excess lithium and potassium triethylborohydrides are used in the photodoping, formation of Zn^0 is observed. The relationship between metallic Zn^0 formation and ZnO surface electron traps is discussed.

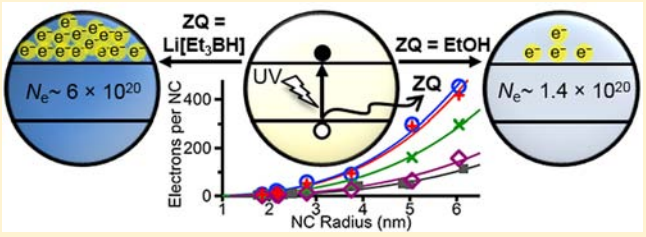

INTRODUCTION

The introduction of extra charge carriers into free-standing colloidal semiconductor nanocrystals constitutes a long-standing challenge in the development of nanocrystal building blocks for quantum dot solar cells, transistors, photodetectors, and electroluminescent devices. Successful strategies for introducing extra band-like charge carriers into colloidal semiconductor nanocrystals have included remote doping,[1,2] defect- or vacancy-induced doping,[3,4] photochemical[2,5−10] or electrochemical reduction,[7,11−13] and aliovalent doping.[10,14−16] Among free-standing colloidal nanocrystals, the extra electrons of reduced colloidal ZnO nanocrystals are arguably the most extensively investigated.[1,2,5−10,17] Most commonly, these electrons have been generated by photochemical oxidation of ethanol (EtOH),[5,6,8−10,17] as described by eq 1.[18−20] UV illumination of ZnO nanocrystals excites an electron across the band gap and, in the presence of EtOH or other hole quenchers (ZQ), the photogenerated valence-band hole (h^+_{VB}) can be captured irreversibly. This chemistry deposits conduction-band electrons (e^-_{CB}) and charge-compensating protons or other cations (Z^+). Remarkably, extended UV irradiation leads to accumulation of multiple conduction-band electrons per colloidal ZnO nanocrystal (Scheme 1).[6,9] Under rigorously anaerobic conditions, these extra electrons are stable indefinitely, allowing their handling and detailed investigation by physical and chemical techniques.[8,9] Upon exposure to air or other oxidants, these electrons can be removed and the ZnO nanocrystals returned to their original oxidation state. Such chemistry thus offers a postsynthetic method of tuning nanocrystal carrier densities that has proven attractive for numerous physical and chemical investigations.[8−10,17,21−27]

$$e^-_{CB},\ h^+_{VB}\text{: ZnO} + CH_3CH_2OH \rightarrow 2e^-_{CB}\text{: ZnO} + 2H^+ + CH_3CHO \quad (1)$$

Recently, it was demonstrated that photochemical accumulation of multiple conduction-band electrons is made possible by the fact that hole quenching with EtOH is markedly faster than Auger recombination of the charged exciton.[26] Although this observation explains how more than one electron may be injected photochemically, salient questions remain pertaining to the level of electron doping that can be achieved by this method. Previous studies have reported disparate values for the maximum number of electrons per nanocrystal (denoted $\langle n_{max} \rangle$ when averaged over the ensemble) that can be added to colloidal ZnO nanocrystals via photochemical oxidation of EtOH. Titrations have shown $\langle n_{max} \rangle$ = 4 (ref 17), 6 (ref 9), 10 (ref 6), and 48 (ref 10) electrons per ZnO nanocrystal. The cause of this large spread in experimental $\langle n_{max} \rangle$ values has not

Received: August 3, 2013
Published: September 19, 2013

   dx.doi.org/10.1021/ja408030u | J. Am. Chem. Soc. 2013, 135, 16569−16577

Scheme 1

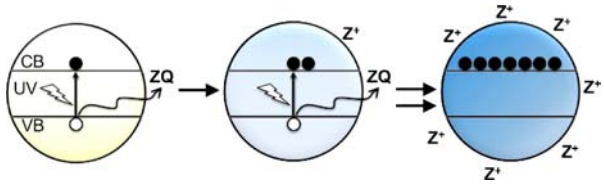

been examined or clarified. Furthermore, the role of the hole quencher in determining $\langle n_{max} \rangle$ has not been examined.

Here, we present a systematic investigation of the maximum number of electrons that can be added to ZnO nanocrystals via photochemical oxidation of EtOH. We demonstrate that $\langle n_{max} \rangle$ varies strongly with nanocrystal radius (r) in a well-behaved fashion, covering nearly 2 orders of magnitude in $\langle n_{max} \rangle$ with only a factor of 4 variation in r. Specifically, $\langle n_{max} \rangle$ is found to scale with nanocrystal volume, yielding nearly constant maximum electron *densities* over all nanocrystal radii. For photodoping using EtOH, $\langle n_{max} \rangle$ is largely independent of solvent, surface-capping ligands, photoexcitation rates, and other experimental variations. We further demonstrate that for a given nanocrystal size, $\langle n_{max} \rangle$ is not intrinsic to the nanocrystal but depends on the specific hole quencher used. We introduce the use of lithium and potassium triethylborohydrides as particularly effective hole quenchers for photodoping ZnO nanocrystals, and demonstrate systematic trends in $\langle n_{max} \rangle$ that relate to the properties of these hole quenchers. Comparison of these hole quenchers with tetrabutylammonium triethylborohydride reveals that the cations can also play an important role in determining $\langle n_{max} \rangle$. These results improve upon existing methods for photodoping ZnO nanocrystals, and shed light onto the fundamental factors governing this nanocrystal photodoping. Ultimately, this knowledge may contribute to the development of new routes to functionalization of colloidal semiconductor nanocrystals for a variety of chemical, optical, or technological applications.

EXPERIMENTAL SECTION

Chemicals. For nanocrystal synthesis, zinc acetate dihydrate ($Zn(OAc)_2$), tetramethylammonium hydroxide pentahydrate (TMAH), dodecylamine (DDA), and trioctylphosphine oxide (TOPO, 90%) were purchased from Sigma-Aldrich and used without further purification.

For photodoping experiments, toluene and THF were obtained from a solvent purification system, transferred to a N_2 glovebox, and placed over molecular sieves for 24 h prior to use. Anhydrous EtOH was purchased from Acros and stored in the glovebox. Lithium triethylborohydride (Li[Et_3BH]), potassium triethylborohydride (K-[Et_3BH]), lithium dimethylaminoborohydride (Li[Me_2NBH_3]), and lithium hexafluorophosphate (Li[PF_6]) were purchased from Sigma-Aldrich as 1 M solutions in THF and stored in the glovebox. Tetrabutylammonium triethylborohydride ([Bu_4N][Et_3BH]) was synthesized by cation exchange. Briefly, 0.1 mmol of [Bu_4N][PF_6] was added to a solution of 0.1 mmol of K[Et_3BH] in 100 μL of THF, and then 100 μL of toluene was added with stirring to precipitate the K[PF_6] byproduct. The resulting solution was filtered through a 200 μm PTFE filter.

For electron-counting experiments, [$FeCp^*_2$][BAr_F] ([$FeCp^*_2$]$^+$ = decamethylferrocenium, [BAr_F]$^-$ = tetrakis[3,5-bis(trifluoromethyl)-phenyl]borate) was synthesized following literature procedures.[28] The starting materials, sodium tetrakis[3,5-bis(trifluoromethyl)phenyl]-borate, bis(pentamethylcyclopentadienyl)iron(II), and iron(III) chloride (99.9%), were purchased from Sigma-Aldrich and used without further purification.

Nanocrystal Synthesis. Colloidal ZnO nanocrystals were synthesized by base-initiated hydrolysis and condensation of Zn^{2+} as detailed previously.[29,30] In a typical synthesis, a solution of 22 mmol of TMAH in 40 mL of EtOH was added dropwise to a stirred solution of 13 mmol of $Zn(OAc)_2$ in 135 mL of DMSO at room temperature. Nanocrystals were grown for 15−45 min, after which the reaction was stopped by precipitation with ∼300 mL of ethyl acetate. Nanocrystals were collected via centrifugation and resuspended in EtOH, followed by precipitation with heptane. To suspend the nanocrystals in nonpolar solvents, the surface ligands were exchanged by suspending the nanocrystals in excess of DDA that had been heated above the melting point (29 °C), followed by precipitation with EtOH. Finally, the nanocrystals were heated in TOPO at 100 °C for 30 min. The resulting TOPO-capped nanocrystals were then washed/resuspended with ∼3:1 EtOH/toluene as described above. Large ZnO nanocrystals were made in a similar manner but were heated under N_2 in DDA at 180 °C for 2−24 h prior to TOPO capping to promote growth to various sizes. Similar photodoping results are obtained for TOPO- and DDA-ligated nanocrystals, but TOPO-ligated nanocrystals retain their solubility better during titrations. We attribute this to the stronger binding of the phosphonate-type ligating groups in the 90% purity TOPO, making it more compatible with the ionic [$FeCp^*_2$][BAr_F] oxidant.

Physical Characterization. NIR absorption spectra were collected in a 1 cm air-free quartz cuvette using a Cary 500 spectrometer, with typical nanocrystal concentrations of 50−100 μM. Band-edge and IR absorption spectra were collected in an air-free CaF_2 IR cell with a 100 μm Teflon spacer using the Cary 500 and a Bruker Vector 33 spectrometer, respectively. All absorption spectra shown are for the same batch of TOPO-capped, r = 2.8 nm nanocrystals suspended in 1:1 toluene/THF. Typical nanocrystal concentrations were 5−30 μM. The radii of small nanocrystals (r < 3.2 nm) were determined from the empirical correlation between radii and absorption spectra.[31] The radii of larger nanocrystals were determined by powder X-ray diffraction (XRD) using a Bruker D8 Discover diffractometer and by statistical analysis of transmission electron microscope (TEM) images collected using a FEI Tecnai G2 F20. Electron paramagnetic resonance (EPR) measurements were collected using a Bruker EMX X-band spectrometer with a SHQE resonater operating at 9.8 GHz. The g values were measured in reference to diphenylpicrylhydrazyl radical (g = 2.0036). For all EPR measurements, the nanocrystals were TOPO-capped and suspended in toluene.

Photodoping. For electron-counting experiments, ZnO nanocrystals suspended in 1:1 toluene/THF were prepared in a 1 cm air-free cuvette and photodoped to their maximum level by prolonged exposure to UV irradiation from a 100 W Hg/Xe Oriel photolysis lamp (∼2 W/cm^2, ∼1.5 cm illumination diameter) in the presence of a reductant. Concentrated aqueous $CuSO_4$ was used as an IR filter to reduce sample heating. Details about the lamp stability are provided in Supporting Information. The NIR absorption was monitored periodically during the photodoping process. When the NIR absorption did not change over ∼20 min of UV exposure, the nanocrystals were considered to have reached their maximum photodoping level. Under these conditions, maximum photodoping levels were typically reached within 2−4 h without stirring.

For photodoping using EtOH, ZnO nanocrystals were suspended in anaerobic toluene/THF (1:1) solutions at the nanocrystal concentrations described above. THF was used to aid the solubility of [$FeCp^*_2$][BAr_F] during titrations[17] (see below). Photodoping in the presence of EtOH was performed on both TOPO- and DDA-capped nanocrystals.

For photodoping using the hydride hole quenchers, solutions were prepared the same way, with the addition of ∼100−500 equiv of hydride. As discussed below, photodoping with the hydrides, especially Li[Et_3BH] and Li[Me_2NBH_3], sometimes resulted in formation of a brown/black byproduct that showed an XRD pattern consistent with that of Zn^0 metal (see Supporting Information for details). The formation of this byproduct could be greatly reduced by periodically adding the hydride in small (∼10−50 equiv) aliquots during the

dx.doi.org/10.1021/ja408030u | J. Am. Chem. Soc. 2013, 135, 16569−16577

photodoping process instead of introducing the entire amount at once so as to keep the unused hydride concentration low.

For kinetic measurements, TOPO-capped r = 2.8 nm nanocrystals suspended in 1:1 toluene/THF were used. Nanocrystal solutions were prepared to contain ∼5 μM nanocrystals. The samples photodoped using hydrides were prepared with ∼500 equiv of hydride. The samples photodoped using EtOH and EtOH/Li[PF_6] were prepared with ∼2×10^4 equiv of EtOH and ∼2×10^4 equiv of EtOH plus ∼500 equiv of Li[PF_6], respectively. All samples were stirred while irradiating.

For IR measurements, nanocrystals were photodoped in situ in an air-free IR cell. ZnO nanocrystal solutions were prepared as described above, kept in the dark, and used for background measurements. The samples were then exposed to UV irradiation and the IR spectra measured until they stopped changing. Under these conditions, maximum photodoping levels were typically reached within 10−120 s. Prolonged UV irradiation after reaching the maximum photodoping level causes some irreversible photochemistry, manifested as diminished red shift in the IR absorption during reoxidation, attributed to poor mixing in the IR cell.

Electron Counting. The average number of excess electrons per ZnO nanocrystal ($\langle n \rangle$) photodoped using EtOH was determined by titration with [$FeCp^*_2$][BAr_F].[10,17] Aliquots of [$FeCp^*_2$][BAr_F] in THF were added to the maximally photodoped nanocrystals and the reduction of the NIR absorption was monitored. After complete elimination of the NIR absorption, additional aliquots led to growth of [$FeCp^*_2$]$^+$ absorption centered at ∼700 nm. Further details and titration data are provided in the Supporting Information. For the other hole quenchers, $\langle n \rangle$ was determined ratiometrically by comparing their NIR absorption (integrated between 800 and 1400 nm, far in the high-energy tail of the IR absorption band) with that of the same nanocrystals photodoped using EtOH (see Supporting Information for details). In select cases, these reduced nanocrystals were also titrated against [$FeCp^*_2$][BAr_F], and good agreement between the titration and ratiometric optical methods was observed. All size-dependent electron-counting data presented in the main text were fit in original (linear) form. For fits obtained using the log−log form of the data, see Supporting Information.

Identification of Zn^0. The formation of metallic Zn^0 was observed following prolonged UV exposure (24 h) in the presence of a large excess of Li[Et_3BH] (∼3×10^4 equiv). The resulting black, cloudy solution was centrifuged and the ZnO nanocrystals could be washed away with hexanes while the black pellet would not resuspend. The black pellet was dried and pressed between two pieces of Kapton tape for XRD analysis.

RESULTS AND ANALYSIS

Figure 1 shows UV/vis, IR, and EPR spectra of colloidal r = 2.8 nm ZnO nanocrystals collected before and after various durations of UV exposure in the presence of EtOH. As reported previously,[2,9] electron accumulation is accompanied by a bleach of the band edge absorption (Figure 1a), corresponding to filling of the conduction band, and by growth of an intense absorption band in the IR (Figure 1b) attributable to intra-conduction-band transitions. With electron accumulation, the IR band increases in intensity and shifts to higher energy. The appearance of an EPR signal at $g \approx 1.96$ (Figure 1c), and its dependence on nanocrystal radius,[21] confirms that these extra electrons are delocalized in the conduction band. This photodoping is completely reversed upon exposure of the nanocrystals to air or other appropriate oxidants, returning the spectroscopic properties to their original values.

Photodoping experiments were performed on colloidal ZnO nanocrystals with average radii ranging from r = 1.75 to 6.15 nm using EtOH as the hole quencher. For each sample, $\langle n_{max} \rangle$ was determined by titration against [$FeCp^*_2$][BAr_F].[10,17] Figure 2a presents a double-log plot of the resulting $\langle n_{max} \rangle$ values (blue squares) vs nanocrystal radius. The entire data set spans nearly 2 orders of magnitude in $\langle n_{max} \rangle$, showing a strong and well-behaved dependence on nanocrystal radius. The present data agree remarkably well with data reported in previous studies of ZnO nanocrystals in which EtOH was the hole quencher (red circles).[6,9,10,17] This data set includes nanocrystals with amine, TOPO/phosphonate, or acetate/hydroxide surface-capping ligands that are suspended in toluene, toluene/THF, or EtOH solvents (see Supporting Information for details). Photolysis was performed at different nanocrystal concentrations with different excitation rates and in different laboratories. Nevertheless, all of these data fall on the same line in Figure 2a, indicating that $\langle n_{max} \rangle$ is not particularly sensitive to precise experimental conditions such as solvent, ligands, photolysis conditions, and nanocrystal or EtOH concentrations. The disparate literature values thus follow a rational and fundamentally meaningful trend. Fitting these data to a phenomenological power law expression (eq 2) yields the solid black line plotted in Figure 2a with a best-fit exponential value of p = 2.8 ± 0.2. For comparison, the dashed line in

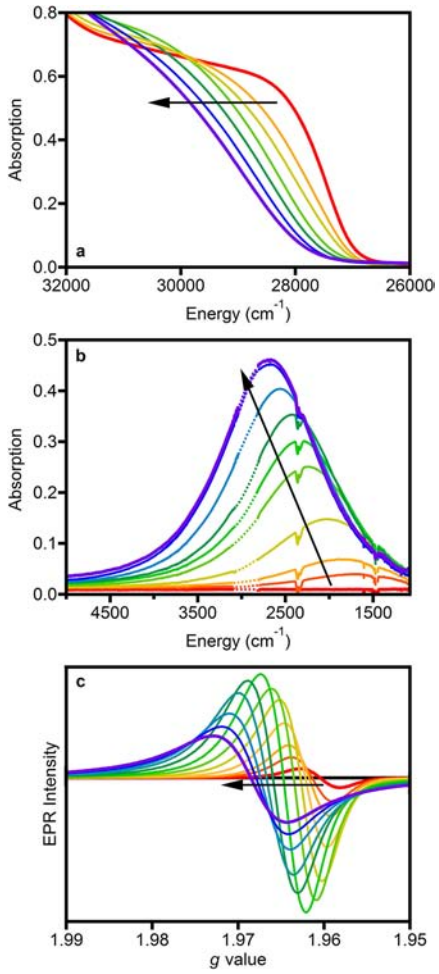

Figure 1. Representative spectroscopic signatures of photodoping in colloidal ZnO nanocrystals. Photochemical addition of conduction-band electrons leads to (a) a bleach in the UV absorption, (b) growth of IR absorption, and (c) appearance of a $g \approx 1.96$ EPR signal. The arrows indicate increased UV irradiation time. The region of intense ligand and solvent C−H stretches (∼2800−3100 cm^{-1}) in panel (b) has been interpolated for clarity (dotted lines). Spectra are shown for ∼10 μM in 1:1 toluene/THF (absorption) and ∼100 μM in toluene (EPR) colloidal TOPO-capped r = 2.8 nm ZnO nanocrystals.

dx.doi.org/10.1021/ja408030u | J. Am. Chem. Soc. 2013, 135, 16569−16577

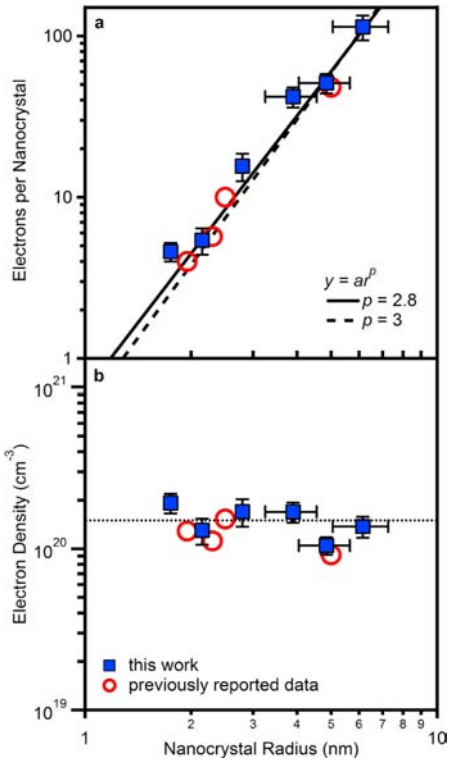

Figure 2. Size dependence of the maximum photodoping level in colloidal ZnO nanocrystals using EtOH as the hole quencher. (a) Average maximum number of electrons per nanocrystal ($\langle n_{max} \rangle$) plotted vs nanocrystal radius on logarithmic scales. The solid blue squares are data points from the present study. The red open circles show literature data points, one each from refs 6, 9, 10, and 17. The solid line represents the best fit to eq 2, which yields p = 2.8. The dashed line shows the best fit for p = 3.0. (b) The data from (a) replotted as the average maximum electron density ($\langle N_{max} \rangle$) vs nanocrystal radius on logarithmic scales. The dotted line is the maximum electron density averaged over all nanocrystal sizes ($\langle \langle N_{max}^{EtOH} \rangle \rangle$ = (1.4 ± 0.4) × 10^{20} cm^{-3}).

Figure 2a shows the best fit obtained when fixing p = 3.0, demonstrating that $\langle n_{max} \rangle$ varies roughly in proportion to the nanocrystal volume. As a consequence of this size dependence, the average maximum electron *density* ($\langle N_{max} \rangle$) remains essentially constant across this entire set of samples. To illustrate this point, Figure 2b plots the data from Figure 2a as $\langle N_{max} \rangle$ vs nanocrystal radius. All nanocrystals display similar maximum electron densities of $\langle N_{max} \rangle \approx (1-2) \times 10^{20}$ cm^{-3}. The dashed line represents the average value of $\langle N_{max} \rangle$ over all sizes of nanocrystals, $\langle \langle N_{max}^{EtOH} \rangle \rangle$ = (1.4 ± 0.4) × 10^{20} cm^{-3}.

$$\langle n_{max} \rangle = ar^p \tag{2}$$

To date, the influence of the hole quencher on $\langle n_{max} \rangle$ in colloidal ZnO nanocrystals has not been explored. To investigate this variable, colloidal ZnO nanocrystals were photoexcited in the presence of four additional hole quenchers, defined here as ZQ. These hole quenchers included two different anions (Q^-): triethylborohydride and dimethylaminoborohydride ($[Et_3BH]^-$ and $[Me_2NBH_3]^-$, respectively). For the $[Et_3BH]^-$ anion, three different charge-compensating cations (Z^+) were investigated: Li^+, K^+, and tetrabutylammonium ($[Bu_4N]^+$). Similar to EtOH, the hydrides successfully quench photogenerated holes and lead to electron accumulation in ZnO nanocrystals photoexcited under anaerobic conditions. For these hole quenchers, the net photochemical reactions are not yet known, but we speculate that they may be summarized as shown in eq 3, where Z^+ represents Li^+, K^+, or $[Bu_4N]^+$. This representation assumes "current doubling" analogous to that reported for EtOH (eq 1),[18,20] but current doubling with these hydride hole quenchers has not been confirmed. The results presented below do not rely on any assumptions about current doubling.

$$e_{CB}^-, h_{VB}^+: \text{ZnO} + \text{Z}[Et_3BH] \rightarrow 2e_{CB}^-: \text{ZnO} + H^+ + Z^+ + BEt_3 \tag{3a}$$

$$e_{CB}^-, h_{VB}^+: \text{ZnO} + \text{Li}[Me_2NBH_3] \rightarrow 2e_{CB}^-: \text{ZnO} + H^+ + Li^+ + Me_2NBH_2 \tag{3b}$$

Figure 3a shows IR absorption spectra of r = 2.8 nm nanocrystals after maximum photodoping in the presence of EtOH, $Li[Et_3BH]$, $K[Et_3BH]$, $[Bu_4N][Et_3BH]$, or $Li[Me_2NBH_3]$. These experiments demonstrate that $\langle n_{max} \rangle$ can be markedly increased by changing the hole quencher. Figure 3b plots the $\langle n_{max} \rangle$ values obtained using the various hole quenchers as a function of nanocrystal radius. As with EtOH in Figure 2, $\langle n_{max} \rangle$ is a strong function of nanocrystal radius for each hole quencher, in every case changing roughly in proportion to the nanocrystal volume. For the hydrides, fits of these data to eq 2 all yield values of p close to 3 (see Supporting Information). The solid lines in Figure 3b show fits

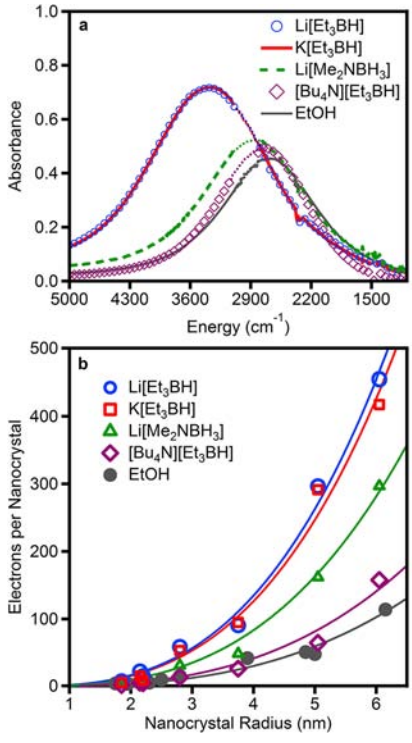

Figure 3. (a) IR absorption of colloidal r = 2.8 nm ZnO nanocrystals (TOPO-capped in 1:1 toluene/THF) photodoped in the presence of EtOH (solid gray line), $[Bu_4N][Et_3BH]$ (purple diamonds), $Li[Me_2NBH_3]$ (dashed green line), $K[Et_3BH]$ (solid red line) and $Li[Et_3BH]$ (blue circles) hole quenchers. The region of intense ligand and solvent C−H stretches (~2800−3100 cm^{-1}) has been interpolated for clarity (dotted lines). (b) Size dependence of $\langle n_{max} \rangle$ of ZnO nanocrystals photodoped using the hole quenchers from (a). The solid lines show fits to eq 2 in which p is fixed to 3.0.

dx.doi.org/10.1021/ja408030u | J. Am. Chem. Soc. 2013, 135, 16569−16577

obtained with p fixed to a value of 3.0. This fitting allows meaningful information to be extracted from the coefficient a: The ratio of a^{ZQ} to a^{EtOH} represents the maximum photodoping achieveable with the various hydride hole quenchers, relative to EtOH. Multiplying this ratio by $\langle\langle N_{max}^{EtOH}\rangle\rangle$ thus yields $\langle\langle N_{max}^{ZQ}\rangle\rangle$. The results of this fitting are summarized in Table 1. Floating p yields slightly different values but the same trend (see Supporting Information).

To test whether the high carrier densities achieved with some hydrides still involve delocalized electrons, EPR measurements were performed. Figure 4a shows the EPR spectra of colloidal r = 2.15 nm ZnO nanocrystals at various stages of UV irradiation in the presence of Li[Et_3BH]. As with ZnO nanocrystals photodoped using EtOH (Figure 1c), increased UV irradiation causes an increase in g value and a broadening of the EPR signal.[9] Figure 4b plots EPR spectra of the same ZnO nanocrystals photodoped to their maximum extent using EtOH or Li[Et_3BH] as the hole quencher. Consistent with the absorption experiments, the higher g value and broader line width of the latter confirms that photodoping using Li[Et_3BH] as the hole quencher yields higher densities of conduction-band electrons in colloidal ZnO nanocrystals.

To gain further insight into the reactivity of the borohydride hole quenchers, electron accumulation kinetics were measured with various hole quenchers. Anaerobic solutions of r = 2.8 nm ZnO nanocrystals were prepared in the presence of each hole quencher and exposed to UV illumination under identical conditions. Figure 5a plots the relative NIR absorption intensities ($A_{photodoped} - A_{as\text{-}prepared}$ at 1400 nm) as a function of UV irradiation time. For a given sample, these values are directly proportional to the average number of accumulated electrons per nanocrystal, $\langle n\rangle$. In all cases, $\langle n\rangle$ increases rapidly before leveling off at $\langle n_{max}\rangle$. A salient observation from these measurements is that photodoping with the hydride hole quenchers reaches $\langle n_{max}\rangle$ much more quickly than with EtOH, despite the fact that EtOH is added at concentrations ~40 times greater than the hydrides in these experiments. To test if the difference in rates between the hydrides and EtOH may simply relate to the addition of cations such as Li^+, parallel photodoping measurements were performed using EtOH with added Li[PF_6]. The addition of Li[PF_6] has only a minor effect on the ZnO photodoping kinetics and no effect on $\langle n_{max}\rangle$ (Figure 5a). Similarly, addition of the acid [$H(Et_2O)_2^+$][$BArF_4^-$] before or during photodoping has no effect on $\langle n_{max}\rangle$ (see Supporting Information). The difference between the hydrides and EtOH is also not linked to the absolute magnitude of $\langle n_{max}\rangle$, because [Bu_4N][Et_3BH] and EtOH yield very similar $\langle n_{max}\rangle$ values even though photoreduction is much faster when using [Bu_4N][Et_3BH]. We note that both EtOH curves in Figure 5a show a small amount (~10%) of rapid photodoping within the first 30 s, followed by slower photodoping over the course of many minutes.

Table 1. Summary of the Size Dependence of ZnO Nanocrystal Photodoping Using Various Hole Quenchers (ZQ)[a]

ZQ	a	a^{ZQ}/a^{EtOH}	$\langle\langle N_{max}^{ZQ}\rangle\rangle$ ($\times 10^{20}$ cm^{-3})
EtOH	0.5	1	1.4
[Bu_4N][Et_3BH]	0.7	1.4	2.0
Li[Me_2NBH_3]	1.3	2.7	3.8
K[Et_3BH]	2.0	4.1	5.7
Li[Et_3BH]	2.1	4.4	6.1

[a]These parameters were obtained by fitting the data of Figure 3b to eq 2 with p fixed at 3.0. Here, a^{ZQ} is the scaling coefficient (proportional to $\langle\langle N_{max}\rangle\rangle$) and a^{ZQ}/a^{EtOH} represents the scaling coefficient relative to EtOH. The maximum photodoping was calculated as $\langle\langle N_{max}^{ZQ}\rangle\rangle = (a^{ZQ}/a^{EtOH})\langle\langle N_{max}^{EtOH}\rangle\rangle$, with $\langle\langle N_{max}^{EtOH}\rangle\rangle = (1.4 \pm 0.4) \times 10^{20}$ cm^{-3}. Typical errors in a are small ($<\pm 0.1$), and all uncertainties in $\langle\langle N_{max}^{ZQ}\rangle\rangle$ are thus estimated to be within ~30% based on the uncertainty in $\langle\langle N_{max}^{EtOH}\rangle\rangle$.

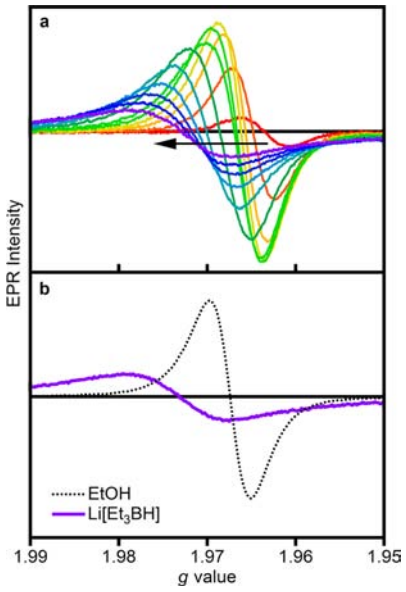

Figure 4. EPR spectra of photochemically reduced colloidal r = 2.15 nm TOPO-capped ZnO nanocrystals in toluene. (a) Spectra recorded at various stages of UV irradiation in the presence of Li[Et_3BH]. (b) Comparison of the same nanocrystals photoreduced to the maximum extent using EtOH (dotted black line) or Li[Et_3BH] (solid purple line) as the hole quencher.

To quantify the above observations, the data in Figure 5a were fit to a double-exponential function (dotted lines) to extract initial photodoping rates ($R_0 = (dA/dt)|_{t=0}$) and asymptotic absorbance values (A_{max}, which represents the absorbance at $\langle n_{max}\rangle$).[32] The trends in these two parameters are largely insensitive to the precise form of the fitting function (e.g., bi- vs multiexponential). The details of this analysis are provided in the Supporting Information, and the results are summarized in Table 2. The ratio $A_{max}^{ZQ}/A_{max}^{EtOH}$ in Table 2 reflects the ratio $\langle N_{max}^{ZQ}\rangle/\langle N_{max}^{EtOH}\rangle$ for these measurements and is analogous to the data of Figure 3b summarized in Table 1, except not averaged over multiple nanocrystal radii and measured at only one absorption wavelength. The trends summarized in Table 2 capture (i) the faster photodoping achieved with all of the hydrides relative to EtOH and (ii) the greater photodoping levels achieved with some hydrides relative to EtOH. Although R_0 increases rapidly from EtOH to [Bu_4N][Et_3BH] and Li[Me_2NBH_3], there is no corresponding increase in $A_{max}^{ZQ}/A_{max}^{EtOH}$. Among the hydrides alone, however, R_0 and A_{max} ($\langle N_{max}\rangle$) appear strongly correlated. To illustrate this point, Figure 5b plots R_0^{ZQ}/R_0^{EtOH} vs $A_{max}^{ZQ}/A_{max}^{EtOH}$ for each hole quencher. The hydride data all fall onto the same line, whereas the EtOH data lie well below this line.

Finally, we note the observation of Zn^{2+} reduction to form metallic Zn^0 when photodoping is performed in the presence of excess Li[Et_3BH], Li[Me_2NBH_3], and to lesser extent, K[Et_3BH] hole quenchers. Zn^0 is not observed when photodoping is performed in the presence of excess EtOH or

dx.doi.org/10.1021/ja408030u | J. Am. Chem. Soc. 2013, 135, 16569−16577

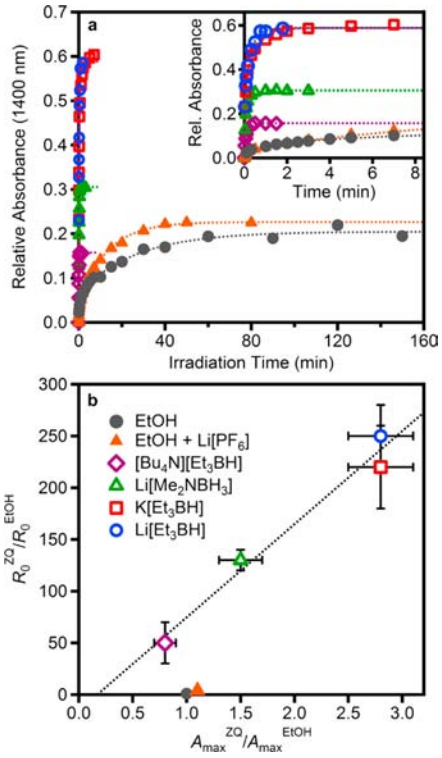

Figure 5. (a) Photodoping kinetics for colloidal r = 2.8 nm ZnO nanocrystals (TOPO-capped in 1:1 toluene/THF) irradiated with UV light in the presence of EtOH (filled gray circles), $[Bu_4N][Et_3BH]$ (open purple diamonds), $Li[Me_2NBH_3]$ (open green triangles), $K[Et_3BH]$ (open red squares), $Li[Et_3BH]$ (open blue circles), and EtOH with added $Li[PF_6]$ (open orange triangles). All solutions had the same nanocrystal concentration (~5 μM). The dashed lines show double-exponential fits to the data. (b) Plot of R_0^{ZQ}/R_0^{EtOH} vs $A_{max}^{ZQ}/A_{max}^{EtOH}$ for EtOH (closed symbols) and hydride (open symbols) hole quenchers. The dotted line is a linear fit to the hydride data. Hydride and $Li[PF_6]$ concentrations were ~500 equiv per nanocrystal, while EtOH concentrations were ~2×10^4 equiv per nanocrystal.

Table 2. Summary of the Time Dependence for Colloidal r = 2.8 nm ZnO Nanocrystal Photodoping in the Presence of Various Hole Quenchers, Based on Analysis of the Data in Figure 5a

ZQ	R_0^{ZQ}/R_0^{EtOH}	$A_{max}^{ZQ}/A_{max}^{EtOH}$
EtOH	1	1
EtOH + $Li[PF_6]$	4 ± 1	1.1 ± 0.1
$[Bu_4N][Et_3BH]$	50 ± 20	0.8 ± 0.1
$Li[Me_2NBH_3]$	130 ± 10	1.5 ± 0.2
$K[Et_3BH]$	220 ± 40	2.8 ± 0.3
$Li[Et_3BH]$	250 ± 30	2.8 ± 0.3

$[Bu_4N][Et_3BH]$. The formation of a metallic species was noticed by a brown/black coloration of the ZnO nanocrystal suspensions upon photolysis (see Supporting Information). Considerably more coloration is observed when UV photodoping is performed in the presence of a large excess of hydride compared to when small aliquots of hydride are titrated in during the photodoping process. Within experimental uncertainty, the same value of $\langle n_{max} \rangle$ was achieved for any given hole quencher, regardless of how much coloration was observed. The coloration was not reversed by exposure to O_2. Under the conditions used for the data presented above, metallic Zn^0 could not be detected analytically, for example by XRD or TEM, suggesting its presence in trace quantities. Eventually, metallization was confirmed by XRD of samples exposed to prolonged UV irradiation (24 h) in the presence of a very large excess of $Li[Et_3BH]$ (>10^4 equiv, see Supporting Information). These conditions are extreme compared to those used for the data presented above (~3−10 min irradiation with ≤500 equiv of hydride). The collected byproduct showed sharp XRD peaks attributable to relatively large Zn^0 metal particles, as well as weaker, similarly sharp peaks that were unidentifiable but may reflect formation of a Li_xZn intermetallic similar to that observed following electrochemical reduction of ZnO nanowires in the presence of Li^+.[33]

DISCUSSION

The data presented above allow three primary conclusions to be drawn about colloidal ZnO nanocrystal photodoping: (i) Photodoping using EtOH as the hole quencher shows a strong volume dependence and no evident dependence on other experimental variables (ligand, solvent, concentration, photolysis conditions, added cations, luminescence quantum yield), such that the entire collection of present and literature data is described well by a single average maximum electron density of $\langle\langle N_{max}^{EtOH} \rangle\rangle = (1.4 \pm 0.4) \times 10^{20}$ cm^{-3}. (ii) Similar volume dependence is observed with other hole quenchers (ZQ), but $\langle\langle N_{max} \rangle\rangle$ depends on ZQ and can be increased substantially by switching from EtOH to $Li[Et_3BH]$ or $K[Et_3BH]$. (iii) Under specific photodoping conditions, metallic Zn^0 is formed, indicating electron localization that appears to be aided by Li^+ and, to a lesser extent, K^+.

The strong dependence of $\langle n_{max} \rangle$ on volume when using EtOH as the hole quencher, and its weak dependence on other experimental parameters, is a central result from this work that raises fundamental questions about the microscopic origins of this doping limit in ZnO nanocrystals. Bulk ZnO shows a similar n-type doping limit ($\langle N_{max} \rangle \approx 10^{21}$ cm^{-3}),[34] which has been proposed to arise from enhanced formation of compensating Zn^{2+}-vacancy centers under heavy n-type aliovalent doping conditions.[35] Analogously, in ZnO nanocrystals, n-doping by Al^{3+} substitution may be viewed as being limited by the capacity of localized surface charges to compensate the aliovalent dopants.[10] Nanocrystal photodoping, however, is likely limited by the photoprocesses themselves. Reaching an $\langle n_{max} \rangle$ means that the net photodoping probability decreases to zero as $\langle n \rangle$ (or $\langle N \rangle$) increases.

As discussed previously,[2,26] one possible photophysical origin of $\langle n_{max} \rangle$ in photodoped ZnO nanocrystals could be the competition between hole quenching and multicarrier Auger recombination. For example, after successful addition of one extra conduction-band electron to a ZnO nanocrystal, the addition of a second electron must proceed via a negative trion. If trion Auger recombination occurs before the valence band hole is transferred to the hole quencher, a second electron will not be accumulated in the nanocrystal. A similar competition applies to quenching of trapped holes.[27] Thus, to add more than one e_{CB}^- per nanocrystal, hole quenching must compete kinetically with multicarrier Auger recombination. Because multicarrier Auger recombination rates increase with the number of excess charge carriers,[36] Auger recombination should become progressively more competitive with hole quenching and could thus determine $\langle n_{max} \rangle$. Recently, however, it was shown that hole capture by EtOH is roughly an order of magnitude faster (<15 ps) than trion Auger recombination (~150 ps, ref 37, both size dependent) and should therefore be

dx.doi.org/10.1021/ja408030u | J. Am. Chem. Soc. 2013, 135, 16569−16577

kinetically competent for the accumulation of multiple conduction-band electrons.[26] Furthermore, the exciton lifetime was shown to *increase* with increasing $\langle n \rangle$, all the way up to $\langle n_{max} \rangle$,[26] whereas exciton lifetimes limited by multicarrier Auger recombination would decrease with increasing $\langle n \rangle$. Consequently, we conclude that $\langle n_{max} \rangle$ is not limited solely by multicarrier Auger recombination.

A second possibility is that $\langle n_{max} \rangle$ is determined primarily by the properties of the hole quencher, ZQ. This possibility was investigated by using Li[Et_3BH], K[Et_3BH], Li[Me_2NBH_3], and [Bu_4N][Et_3BH] in place of EtOH. For a given nanocrystal sample, $\langle n_{max} \rangle$ could be increased more than 4-fold by using a more reactive hole quencher. Thus, $\langle n_{max} \rangle$ clearly depends on the identity of ZQ. Moreover, the data suggest that both the anionic (Q^-) and cationic (Z^+) portions of ZQ influence photodoping. For example, $[Et_3BH]^-$ is a common reducing agent whose alkyl electron-donating groups make it more reducing than an unsubstituted borohydride. Conversely, the electron-withdrawing nitrogen of $[Me_2NBH_3]^-$ makes this species less reducing than an unsubstituted borohydride. Both of these hydrides are expected to be much better reductants than EtOH. Based on these qualitative considerations, the trend in $\langle n_{max} \rangle$ for a given ZnO sample could be anticipated to be $[Et_3BH]^- > [Me_2NBH_3]^- >$ EtOH, which agrees well with the experimental trend of Li[Et_3BH] ≈ K[Et_3BH] > Li[Me_2NBH_3] > EtOH (Table 1). This correlation indicates that $\langle n_{max} \rangle$ is in some way affected by the strength of Q^- as a reductant. Still, the effect is relatively modest, with only 3 times higher $\langle n_{max} \rangle$ for Li[Et_3BH] than for EtOH despite the much greater reducing power of the borohydride.

The outlier in the above trend is [Bu_4N][Et_3BH], which is unable to reduce the nanocrystals to the same extent as its Li^+ and K^+ counterparts can and is only slightly more effective than EtOH. This result indicates that the cations also play an important role. On one hand, the smaller $\langle n_{max} \rangle$ obtained with [Bu_4N][Et_3BH] could be attributed to poorer stabilization of ZnO electrons by the bulky $[Bu_4N]^+$ cation. This interpretation would be consistent with the greater effect of Li^+ than $[Bu_4N]^+$ on the band-edge energies of bulk ZnO. It is also consistent with recent work demonstrating greater chemical reduction of ZnO nanocrystals when using protons rather than bulky metallocene cations for electron charge compensation.[38] It is conceivable, however, that the bulky $[Bu_4N]^+$ cation merely limits the effective surface hydride concentration and thereby reduces the probability of hole capture, despite a sufficient thermodynamic driving force.

The insensitivity of $\langle n_{max} \rangle$ to added Li[PF_6] or [$H(Et_2O)^+$][BAr_F] when using EtOH as the hole quencher is a particularly striking result, given the recent demonstration that protons shift colloidal ZnO nanocrystal conduction-band-edge potentials and thereby tune $\langle n_{max} \rangle$ when using chemical reductants such as cobaltocene.[38] A clear conclusion can be drawn that the photochemical $\langle n_{max} \rangle$ is not directly determined by the same equilibrium thermodynamics as the chemical $\langle n_{max} \rangle$. For photodoping, the potentials of the photogenerated holes are probably more relevant than the equilibrium Fermi levels of the reduced nanocrystals, and these holes are likely always sufficiently powerful to oxidize all of the hydrides explored here.

It is noteworthy that all of the hydrides examined here yield substantially faster photochemical electron accumulation than EtOH does (Figure 5a) despite their lower solution concentration. We hypothesize that this faster photodoping reflects greater effective concentrations of the hydrides at the ZnO nanocrystal surfaces compared to EtOH. For example, it is possible that EtOH is only reactive when bound dissociatively to the ZnO surface,[39,40] a condition that would limit its effective concentration. Indeed, Figure 5a shows an initial fast component to photodoping with EtOH (up to ∼10% of A_{max}), followed by slower photodoping for the remaining 90%. This behavior would be consistent with EtOH pre-association and subsequent photodoping rates limited by EtOH configuration. EtOH is thus qualitatively different from the hydrides. When just the hydrides are considered, the initial photodoping rates correlate well with $\langle n_{max} \rangle$ (Figure 5b).

Overall, we conclude that $\langle n_{max} \rangle$ for any given nanocrystal sample is directly determined by ZQ, whereas the volumetric scaling of $\langle n_{max} \rangle$ is universal for all ZQ and hence is intrinsic to the ZnO nanocrystals. One explanation is that $\langle n_{max} \rangle$ is determined primarily by unfavorable hole-capture kinetics at large $\langle n \rangle$, possibly ultimately arising from hole stabilization and contraction due to Coulomb interaction with the multiple accumulated electrons, as described previously.[26]

Finally, we address the formation of metallic Zn^0. The formation of Zn^0 metal has been reported following UV illumination of ZnO sol–gel films[41] and single crystals,[42] accompanied by marked coloration. Black precipitates were also observed in early studies of the photoreduction of ZnO nanocrystals suspended in propanol, and the band-edge absorption bleach upon UV irradiation was therefore initially interpreted entirely in terms of surface Zn^{2+} reduction to Zn^0 metal.[43] It was subsequently recognized by the same authors that delocalized electrons were being stored within the ZnO nanocrystals following photoreduction.[5] The possibility of electron localization in reduced ZnO nanocrystals has since been heavily debated.[7,44,45] The results presented here demonstrate unambiguously that localization of excess electrons in ZnO nanocrystals can occur under specific experimental conditions. Strikingly, Zn^0 forms with only three of our five hole quenchers, and without any apparent correlation to $\langle n_{max} \rangle$. Specifically, only those hole quenchers involving Li^+, and to a far lesser extent K^+, show evidence of Zn^0 formation. Under identical conditions, photodoping with Li[Et_3BH] leads to far more coloration than K[Et_3BH] despite their nearly identical $\langle n_{max} \rangle$, and no coloration is observed with [Bu_4N][Et_3BH]. Likewise, under identical conditions, photodoping with Li[Me_2NBH_3] leads to much more coloration than with K[Et_3BH], despite nearly a factor of 2 smaller $\langle n_{max} \rangle$. Overall, these results implicate the cations of ZQ as noninnocent in the electron-localization process. We hypothesize that Zn^{2+} reduction is facilitated by Li^+ (and to a lesser extent by K^+), which shifts the surface $Zn^{2+/0}$ potential more positive relative to the ZnO conduction-band edge by interacting strongly with surface oxo anions. Li_2O has a greater lattice energy than K_2O, making Zn^0 formation more thermodynamically favorable with Li^+. In support of this interpretation, we note that research into the use of ZnO nanostructures as Li^+ battery anodes[33] has demonstrated that extensive electrochemical reduction in the presence of Li^+ electrolyte severely disrupts the ZnO lattice, eventually converting it to amorphous Li_2O and Zn^0 metal. We propose that similar chemistries occur to a lesser extent under our photochemical reduction conditions when using Li^+-containing hole quenchers.

It remains an open question why more Zn^0 is observed with a large excess of Li[Et_3BH] or K[Et_3BH] compared to when the same quantities of these hole quenchers are added in small aliquots, and why it is not observed in nanocrystals photo-

reduced using EtOH in the presence of $Li[PF_6]$. These observations may implicate an unrelated dark chemical reaction of the hydride. In any case, Zn^0 constitutes a trace side product whose formation appears to be unrelated to $\langle n_{max} \rangle$. Overall, the observation of Zn^0 precipitates under specific photodoping conditions is both cautionary and potentially revealing of the roles of hard Lewis acids in compensating the charges of added electrons in ZnO nanostructures.

CONCLUSION

In summary, the maximum number of kinetically stable, conduction-band electrons that can be added to colloidal ZnO nanocrystals by photochemical oxidation of EtOH increases rapidly with increasing nanocrystal radius, scaling roughly as $\langle n_{max} \rangle \propto r^3$. These numbers are remarkably independent of other experimental parameters. Consequently, ZnO nanocrystals of all radii may be reduced to similar maximum electron *densities* ($\langle\langle N_{max}^{EtOH} \rangle\rangle = (1.4 \pm 0.4) \times 10^{20}$ cm^{-3}) when EtOH is the hole quencher. By switching from EtOH to hydride hole quenchers, $\langle N_{max} \rangle$ can be increased up to $\sim 6 \times 10^{20}$ cm^{-3}. This is a very high value, corresponding to one added electron per ~70 Zn^{2+} ions in the nanocrystal. Work is ongoing to define the structures of these highly reduced nanocrystals, which may be better described as, e.g., $ZnLi_xO$. Further investigation into this chemistry will be of interest both fundamentally and in relation to nanostructured Li^+/ZnO ion battery electrodes. These data suggest that ZnO photodoping limits are determined by the specific identity of ZQ, correlating with the reducing ability of Q^- and influenced by the identity of the countercation. These results are interpreted in terms of competing hole capture and nonproductive recombination channels, a competition that evolves with $\langle n \rangle$. The observation of Zn^0 formation in the presence of Li^+ cations, and to a lesser extent K^+, but not with H^+ or $[Bu_4N]^+$, indicates that electron localization can occur under specific conditions.

The results presented here reconcile the disparate values of electron accumulation reported previously for colloidal ZnO nanocrystals photodoped using EtOH and expand the range of carrier densities achievable in such nanocrystals via photochemical reduction. This ability to tune carrier densities in colloidal semiconductor nanocrystals over a broad range promises to have interesting ramifications in many areas including nanocrystal redox chemistries, nanocrystal doping, and quantum dot plasmonics.

ASSOCIATED CONTENT

Supporting Information

Additional experimental details describing electron counting via chemical titration or ratiometric NIR absorption, additional fits to the size dependence, and pictures showing coloration of nanocrystal suspensions along with XRD of the byproduct. This material is available free of charge via the Internet at http://pubs.acs.org.

AUTHOR INFORMATION

Corresponding Author

gamelin@chem.washington.edu

Notes

The authors declare no competing financial interest.

ACKNOWLEDGMENTS

The authors are grateful to Alicia Cohn and Carolyn Valdez for valuable discussions. We thank the U.S. National Science Foundation (CHE 1151726 to D.R.G. and J.M.M. and Graduate Research Fellowship DGE-0718124 to A.M.S.) for financial support. J.M.M. also acknowledges support from the American Chemical Society Petroleum Research Fund (51178-ND3). This work was funded partially by a Washington NASA Space Grant Consortium Summer Undergraduate Research Fellowship to C.E.G. and by a Department of Energy, Energy Efficiency and Renewable Energy (DOE-EERE) Fellowship to J.D.R. Part of this work was conducted at the University of Washington NanoTech User Facility, a member of the NSF National Nanotechnology Infrastructure Network (NNIN).

REFERENCES

(1) Shim, M.; Guyot-Sionnest, P. *Nature* **2000**, *407*, 981.
(2) Shim, M.; Guyot-Sionnest, P. *J. Am. Chem. Soc.* **2001**, *123*, 11651.
(3) Luther, J.; Jain, P.; Ewers, T.; Alivisatos, A. *Nat. Mater.* **2011**, *10*, 361.
(4) Manthiram, K.; Alivisatos, A. *J. Am. Chem. Soc.* **2012**, *134*, 3995.
(5) Haase, M.; Weller, H.; Henglein, A. *J. Phys. Chem.* **1988**, *92*, 482.
(6) Wood, A.; Giersig, M.; Mulvaney, P. *J. Phys. Chem. B* **2001**, *105*, 8810.
(7) Vanmaekelbergh, D.; Roest, A. L.; Germeau, A.; Kelly, J. J.; Meulenkamp, E. A.; Allan, G.; Delerue, C. *Phys. Rev. Lett.* **2003**, *91*, 169704.
(8) Liu, W. K.; Whitaker, K. M.; Kittilstved, K. R.; Gamelin, D. R. *J. Am. Chem. Soc.* **2006**, *128*, 3910.
(9) Liu, W. K.; Whitaker, K. M.; Smith, A. L.; Kittilstved, K. R.; Robinson, B. H.; Gamelin, D. R. *Phys. Rev. Lett.* **2007**, *98*, 186804.
(10) Schimpf, A. M.; Ochsenbein, S. T.; Buonsanti, R.; Milliron, D. J.; Gamelin, D. R. *Chem. Commun.* **2012**, *48*, 9352.
(11) Wang, C. J.; Shim, M.; Guyot-Sionnest, P. *Science* **2001**, *291*, 2390.
(12) Roest, A. L.; Kelly, J. J.; Vanmaekelbergh, D.; Meulenkamp, E. A. *Phys. Rev. Lett.* **2002**, *89*, 036801.
(13) Guyot-Sionnest, P. *Microchim. Acta* **2008**, *160*, 309.
(14) Kanehara, M.; Koike, H.; Yoshinaga, T.; Teranishi, T. *J. Am. Chem. Soc.* **2009**, *131*, 17736.
(15) Wang, T.; Radovanovic, P. V. *J. Phys. Chem. C* **2011**, *115*, 406.
(16) Buonsanti, R.; Llordes, A.; Aloni, S.; Helms, B.; Milliron, D. *Nano Lett.* **2011**, *11*, 4706.
(17) Schrauben, J.; Hayoun, R.; Valdez, C.; Braten, M.; Fridley, L.; Mayer, J. *Science* **2012**, *336*, 1298.
(18) Markham, M. C.; Hannan, M. C.; Paternostro, R.; Rose, C. B. *J. Am. Chem. Soc.* **1958**, *80*, 5394.
(19) Gomes, W. P.; Freund, T.; Morrison, S. R. *J. Electrochem. Soc.* **1968**, *115*, 818.
(20) Cunningham, J.; Hodnett, B. K. *J. Chem. Soc., Faraday Trans. 1* **1981**, *77*, 2777.
(21) Whitaker, K. M.; Ochsenbein, S. T.; Polinger, V. Z.; Gamelin, D. R. *J. Phys. Chem. C* **2008**, *112*, 14331.
(22) Ochsenbein, S. T.; Feng, Y.; Whitaker, K. M.; Badaeva, E.; Liu, W. K.; Li, X.; Gamelin, D. R. *Nat. Nanotechnol.* **2009**, *4*, 681.
(23) Whitaker, K. M.; Ochsenbein, S. T.; Smith, A. L.; Echodu, D. C.; Robinson, B. H.; Gamelin, D. R. *J. Phys. Chem. C* **2010**, *114*, 14467.
(24) Hayoun, R.; Whitaker, K. M.; Gamelin, D. R.; Mayer, J. M. *J. Am. Chem. Soc.* **2011**, *133*, 4228.
(25) Cohn, A. W.; Kittilstved, K. R.; Gamelin, D. R. *J. Am. Chem. Soc.* **2012**, *134*, 7937.
(26) Cohn, A. W.; Janßen, N.; Mayer, J. M.; Gamelin, D. R. *J. Phys. Chem. C* **2012**, *116*, 20633−20642.
(27) Cohn, A. W.; Schimpf, A. M.; Gunthardt, C. E.; Gamelin, D. R. *Nano Lett.* **2013**, *13*, 1810.
(28) Le Bras, J.; Jiao, H.; Meyer, W. E.; Hampel, F.; Gladysz, J. A. *J. Organomet. Chem.* **2000**, *616*, 54.

(29) Schwartz, D. A.; Norberg, N. S.; Nguyen, Q. P.; Parker, J. M.; Gamelin, D. R. *J. Am. Chem. Soc.* **2003**, *125*, 13205.
(30) Norberg, N. S.; Gamelin, D. R. *J. Phys. Chem. B* **2005**, *109*, 20810.
(31) Meulenkamp, E. A. *J. Phys. Chem. B* **1998**, *102*, 5566.
(32) Strictly speaking, these curves are apparent rates of appearance of conduction-band electrons under the specific photolysis conditions. The relative rates likely mostly reflect the change in photodoping quantum yield as a function of $\langle n_e \rangle$. The relative rates are informative because the photolysis conditions and lamp intensity were kept quite constant over all the experiments, as described in the Supporting Information.
(33) Kushima, A.; Liu, X. H.; Zhu, G.; Wang, Z. L.; Huang, J. Y.; Li, J. *Nano Lett.* **2011**, *11*, 4535.
(34) Agashe, C.; Kluth, O.; Hupkes, J.; Zastrow, U.; Rech, B.; Wuttig, M. *J. Appl. Phys.* **2004**, *95*, 1911.
(35) Noh, J.-Y.; Kim, H.; Kim, Y.-S.; Park, C. H. *J. Appl. Phys.* **2013**, *113*, 153703.
(36) Klimov, V. I.; Mikhailovsky, A. A.; McBranch, D. W.; Leatherdale, C. A.; Bawendi, M. G. *Science* **2000**, *287*, 1011.
(37) Yamamoto, S. *J. Phys. Chem. C* **2011**, *115*, 21635.
(38) Valdez, C. N.; Braten, M.; Soria, A.; Gamelin, D. R.; Mayer, J. M. *J. Am. Chem. Soc.* **2013**, *135*, 8492.
(39) Nagao, M.; Morimoto, T. *J. Phys. Chem.* **1980**, *84*, 2054.
(40) Vohs, J. M.; Barteau, M. A. *Surf. Sci.* **1989**, *221*, 590.
(41) Asakuma, N.; Hirashima, H.; Fukui, T.; Toki, M.; Awazu, K.; Imai, H. *Jpn. J. Appl. Phys.* **2002**, *41*, 3909.
(42) Khan, E. H.; Langford, S. C.; Dickinson, J. T.; Boatner, L. A.; Hess, W. P. *Langmuir* **2009**, *25*, 1930.
(43) Koch, U.; Fojtik, A.; Weller, H.; Henglein, A. *Chem. Phys. Lett.* **1985**, *122*, 507.
(44) Hoyer, P.; Weller, H. *J. Phys. Chem.* **1995**, *99*, 14096.
(45) Shim, M.; Guyot-Sionnest, P. *Phys. Rev. Lett.* **2003**, *91*, 169703.